

Finite difference modelling of near surface effects

Peter M. Manning* and Gary F. Margrave - Dept. of Geology and Geophysics, University of Calgary

CSEG Geophysics 2002

Abstract

A two-dimensional finite-difference modelling program with an accurate free surface representation was used to model dynamite style records. The results depict the recording of near surface effects and their relationships to the recording of body waves. For body waves, the source ghost is shown to cause an approximate derivative wavelet, where the precise phase rotation depends on the depth of the source. The character of the first breaks is shown to depend on the near surface velocity profile, affecting their amplitude, arrival time, and dispersion. The dependence increases as the offset increases. In many cases the effect of the surface ghost and offset dependence of the first breaks can appear to give contradictory polarity results.

Introduction

The study was begun after a series of correspondences with a sponsor of the CREWES project (Sensor Geophysical, Peter Cary) on the use of first breaks to determine polarity of seismic data. The object was to simulate the change of first breaks with offset, and to see if model results would be consistent with the first break polarity determinations commonly assumed. The polarity convention is to plot the first breaks as troughs in order to display positive reflections as peaks. The finite difference modelling was done with the code developed to model surface waves (Manning & Margrave 1999). A staggered grid was used without any correction factors for dispersion or stability.

Model parameters

All models were initiated from a compression source with left/right symmetry at the left edge of the display and so only the right half of the symmetric results were shown. The top of the model was a flat ideal free surface. The bottom of the model was perfectly rigid, and the reflections from it were used as the representation of a positive reflection coefficient. The right edge of the model was affected by code which attempted to eliminate reflections, and succeeded quite well where the velocities next to the edge were the basic uniform velocities of case 1 (described below).

The models used numbers which are realistic as metric units in the earth. The sample rates in the x and z directions were then 2 metres, and the sample rate in time was 0.4 milliseconds. The basic uniform velocities were 1600 m/s for pressure waves and 800 m/s for shear waves. These were modified for later models to provide velocity steps and gradients. The sample rates were fine enough to model the pressure waves accurately, but the surface waves can be seen to have some numerical dispersion.

The energy source was a 30 Hz zero-phase Ricker wavelet applied from zero time at the 0.4 ms sample rate. In order to simulate a compressional source, the displacement specified by the wavelet was applied at the same time to right and left (+x and -x directions) at adjacent sample points. It was also applied down and up (+z and -z directions) at the staggered grid z positions which were symmetric to the x positions (see Figure 1). The displacements applied at a given time were all identical.

The resulting surface recordings are all from vertical geophones. The snapshots within the earth are colour coded to distinguish shear (torque) and pressure events. Pressure events are green/red, and shear events are blue/yellow (Figure 2).

Snapshots at a time halfway through each surface recording give an idea of what is happening within the earth. The events within the earth are coded with three main symbols: R for Rayleigh waves, P for pressure waves, and S for shear waves. The

detailed codes are as follows: Pd for the direct pressure wave, Pr for the bottom reflected pressure wave (with ghost energy), Sg for the shear wave ghost off the surface, Scs for the shear energy converted from the direct pressure wave at the surface, and Scr for the shear wave converted upon reflection at the bottom.

Model results

Case 1: The base model case had the energy source at 8 metres within a uniform velocity field and the surface recording is shown in Figure 3. The zero-phase Ricker wavelet used appears as a first break at zero offset (marked with an R). The reflection at 280 ms. can be seen as a combination of the primary wave at 275 ms. (marked P), and the ghost at 285 ms. (marked G). The brackets show that the effective length of the composite wavelet has not changed much from near offsets to an offset of 350m. The ground roll dispersion is caused mainly by inadequate sampling.

A snapshot of this model at a time of 200 milliseconds is shown in Figure 4. The weak first breaks are at about 270 metres. The compressional reflection Pr is propagating upwards.

Case 2: The second case was identical to the first except that the energy source was placed at 18 metres, and the surface recording is shown in Figure 5. At the left, the Ricker wavelet is again marked with an R, the primary reflection with a P, and the ghost reflection with a G. The primary then appears at shorter time, and the ghost at longer time. The advantage of this deeper shot is reduced ground roll. The disadvantage is that the greater separation of the primary and ghost reflections causes the composite reflection to have a lower frequency and the frequency content to change with offset. This can be seen from the shorter wavelength at the longer offsets for the composite primary/ghost wavelet (shown by the brackets). The change of frequency with offset shown here occurs along shallow reflectors, and the effect is reduced as the depth of the reflectors increase.

The effective change of reflector frequency with offset can cause a significant degradation of statistical deconvolution results. The ghost is then not deconvolved except on near offset traces. A trace at long offsets will have an inconsistent set of frequency lowered reflections, ranging from minimum lowering at shallow times to the equivalent of zero offset lowering at deeper times. This inconsistency severely limits the effectiveness of the deconvolution on these individual traces. A study of this effect with the real Blackfoot data can be seen in Hamarbitan & Margrave (2001).

Inspection of Figures 3 and 5 shows results that are consistent with the standard polarity convention. The first break energy is plotted as a zero phase trough, and the reflection from the positive impedance change is a close approximation to a zero phase peak. The interacting mechanisms to explain this are quite complex, but an important part of the explanation is that the reflection wavelet combines a primary and a ghost.

Case 3: This model has a source at 8 metres as in case 1, but has a velocity gradient of 1600 to 1920 m/sec over a depth range of 20 to 60 metres. This causes the raypaths and wavefronts to curve upward and provides much more energy to the first breaks. A snapshot of the model after 200 milliseconds is shown in Figure 8. The higher energy of the wavefront is shown by the higher colour intensity, and the greater component of energy in the vertical direction results in higher amplitude recording at the vertical geophones.

The surface recording from this model is shown in Figure 7. The higher first break amplitudes at longer offsets are obvious. Close inspection shows a curve toward shorter times with longer offsets, also caused by the velocity gradient. Inspection also shows the first breaks starting to spread out, caused by energy arrival through more than one unique path.

Case 4: This model has the velocity gradient of case 3 and the 18 metre deep shot of case 2. A surface recording is shown in Figure 9 and a snapshot in Figure 10. All the first break characteristics of case 3 can be seen here as well. The first breaks at longer offsets tend to be higher amplitude, more dispersed, and arrive at shorter times because of the velocity gradient.

Case 5: This model is similar to case 3 except that the velocity gradient was replaced by a velocity step, from 1600 to 1920 m/sec. at 40 metres. The shot depth was at 8 metres. The surface recording from this model is shown in Figure 11, and a snapshot in Figure 12.

The features of this model are similar to those of the velocity gradient case of Figure 7 but with several differences. The first break times are not curved, but show an abrupt change in slope at 125 metres. At about the same offset the amplitudes increase, and then show a gradual reduction. It is evident that the first break dispersion is caused by interference between the energy that traveled through the high-speed layer and the remnants of energy that arrived directly through the slower shallow layer.

Multiple reflections also appear, caused by the velocity step. A multiply reflected first break is just beginning to show at the longest offsets. Also a primary reflection is visible at short offsets, and multiples behind the main reflector.

Case 6: This model duplicates the conditions in the earth of case 5 but with the energy source at 18 metres. The surface recording from this model is shown in Figure 13, and the snapshot in Figure 14.

The subtle effects that show in the shallow source of case 5 are also evident in this case. The higher first break amplitudes tend to make the first break multiples more obvious. These are caused by wave packages which reflect between the surface and the higher speed layer at 40 metres. The snapshot also shows a conversion event from this interface.

Conclusions

Finite difference modelling with an accurate free surface representation can give insight into the relationship of the conventional reflections caused by body waves, and the waves affected by boundaries, like first breaks and ground roll. In particular:

- The source ghost causes an apparent phase rotation in the primary reflections relative to the first breaks so that the model results appear to be consistent with the polarity conventions established for standard geophysical processing.
- Reflection character changes dependent on depth of shot can be explained by ghosting, and show how reflections become lower frequency and resist deconvolution application.
- Near surface velocity structure can be related to the first break character changes of amplitude, arrival time, and dispersion.

Acknowledgements

We would like to thank the sponsors of the CREWES project for their generous support.

References

Hamarbitan, N.S. and Margrave, G.F., 2001, Spectral analysis of a ghost: *Geophysics*, **66**, 1267-1273.

Manning, P.M. and Margrave, G.F., 1999, Finite difference modelling as a practical exploration tool: Technical abstracts of 1999 CSEG convention; pp240-243.

Figures

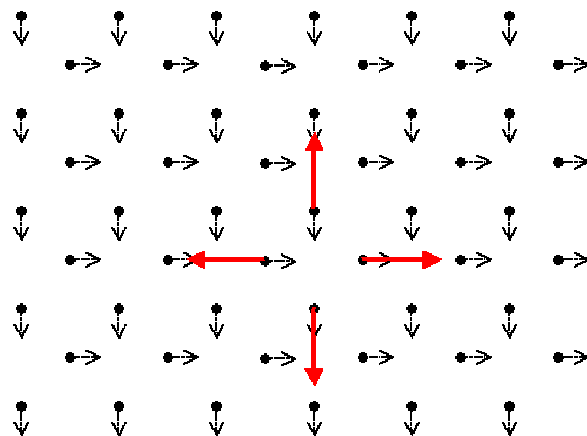


Figure 1: The large arrows show the points within the staggered grid at which the wavelet is applied. The small arrows indicate grid points and the direction of positive displacement within the grid

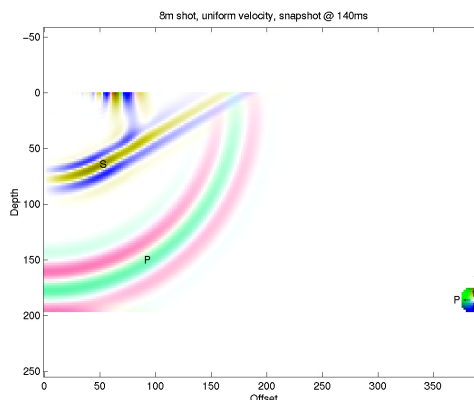


Figure 2: A snapshot from the first model which shows the colour scheme used. P marks a pressure wave colour coded red and green. S marks a shear wave colour coded blue and yellow

Figures

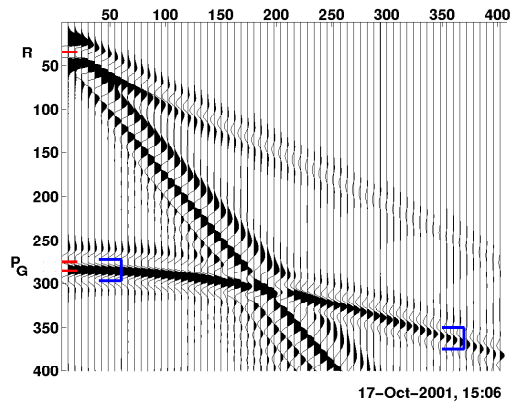


Figure 3: A surface recording of the basic model with an 8 metre source. There is high amplitude ground roll but a high frequency reflection.

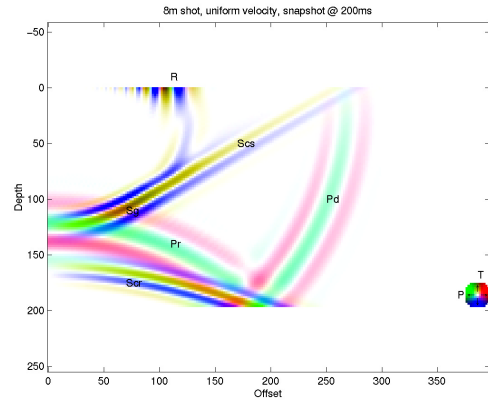


Figure 4: A snapshot of the basic model with an 8 metre source. The three main types of wave are R (Rayleigh), P (Pressure), and S (Shear). See main text for details.

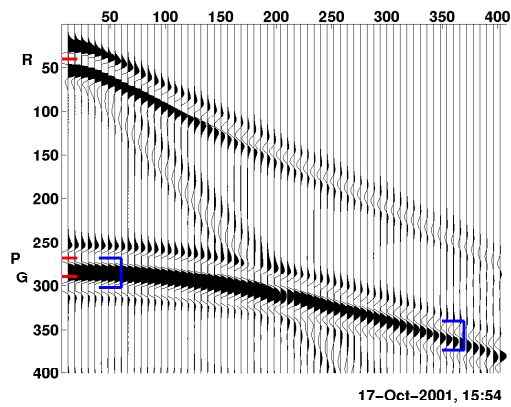


Figure 5: A surface recording of the basic model with a source at 18 metres. The advantage of reduced ground roll is accompanied by the disadvantage of a lower frequency reflection. The reflection is actually a composite of the pressure wave primary and ghost.

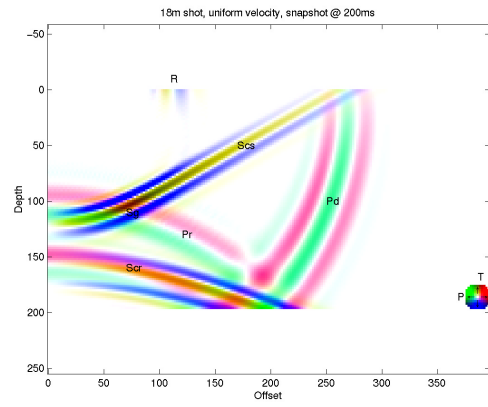


Figure 6: A snapshot of the basic model with the source at 18 metres (case 2).

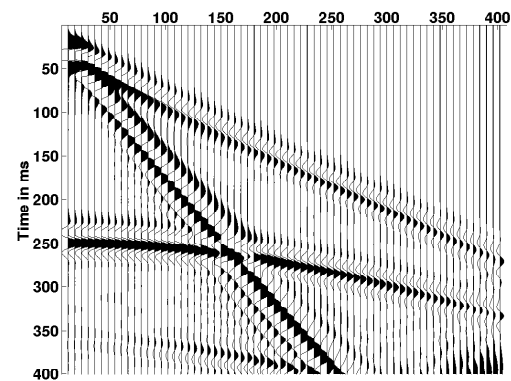


Figure 7: A surface recording from the model of case 3. The first break amplitudes are much higher because of the near surface velocity gradient.

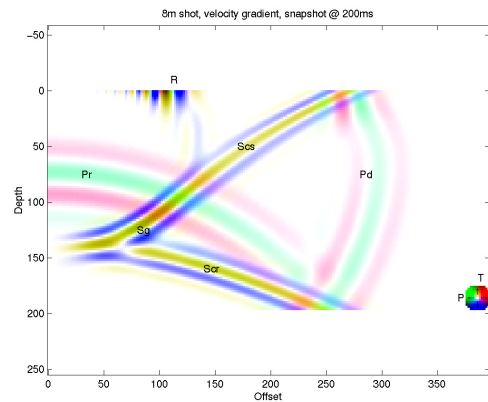


Figure 8: A snapshot of the case 3 model with a near surface velocity gradient. The curved wave propagation caused by the velocity gradient provides much more energy to the first breaks.

Figures

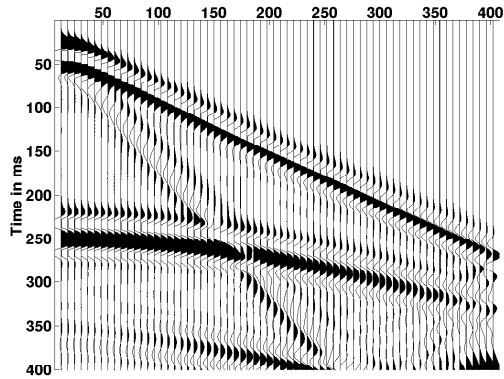


Figure 9: A surface recording from the deep shot model of case 4. First break amplitudes are again higher because of the near surface velocity gradient.

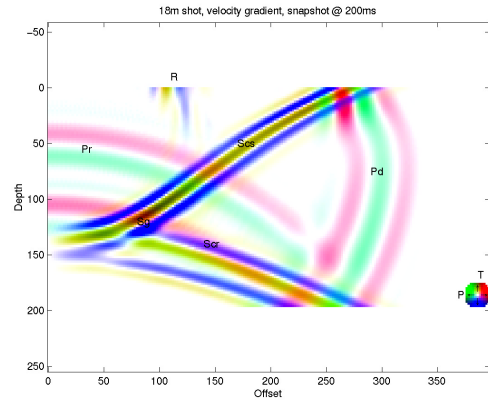


Figure 10: The case 4 snapshot at 200 ms. Again, the upward propagation angle of the direct pressure wave near the surface provides high energy to the first breaks.

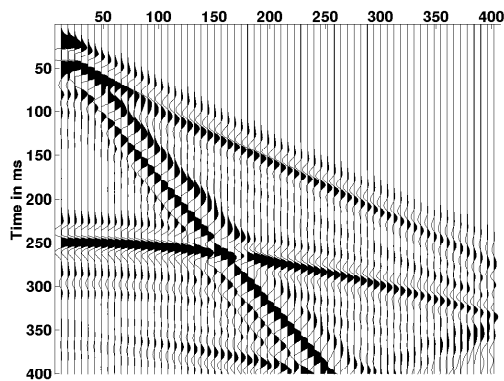


Figure 11: The case 5 model of a shallow shot into the earth with a velocity step at 40 m. Many features are similar to the velocity gradient case

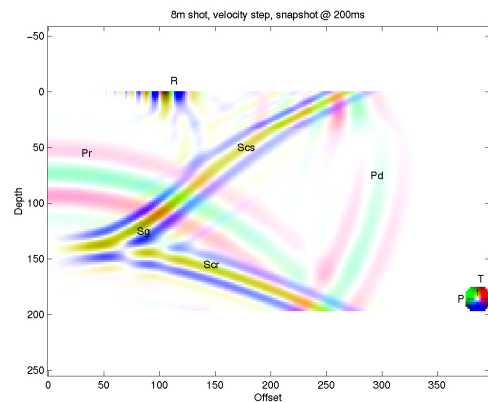


Figure 12: The case 5 snapshot at 200 ms. The similarity to the velocity gradient case can be seen, but multiple energy appears in various places.

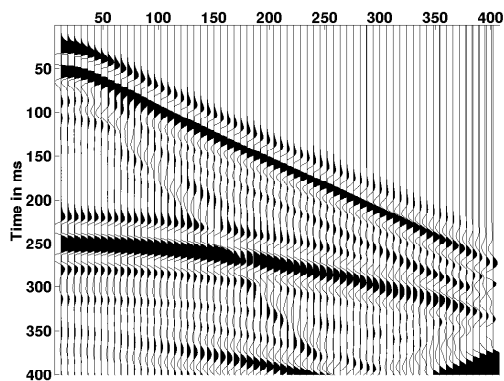


Figure 13: The case 6 model of a deep shot into the earth with the velocity step at 40 m. The higher first break amplitude makes the first break multiple more obvious.

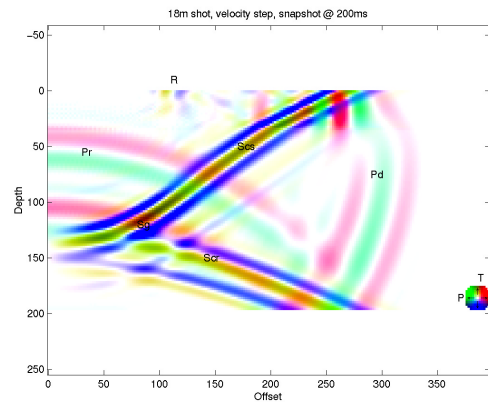


Figure 14: The case 6 snapshot at 200 ms. An additional ghost and P/S conversion from the shallow velocity step can be seen below the surface ghost and conversion.